Solar Energy Materials & Solar Cells 224 (2021) 111016

Contents lists available at ScienceDirect

Solar Energy Materials and Solar Cells

journal homepage: http://www.elsevier.com/locate/solmat

Results on MOVPE SiGeSn deposition for the monolithic integration of III-V and IV elements in multi-junction solar cells

Gianluca Timò [a,b,*], Marco Calicchio [a], Giovanni Abagnale [a], Nicola Armani [a], Elisabetta Achilli [a], Marina Cornelli [a], Filippo Annoni [a], Nicola Castagnetti [b], Maddalena Patrini [b], Lucio Claudio Andreani [b], Lucia Nasi [c], Bernd Schineller [d]

[a] RSE, Strada Torre della Razza, le Mose, 29100, Piacenza, Italy
[b] Department of Physics, University of Pavia, Via Bassi 6, I-27100, Pavia, Italy
[c] IMEM-CNR, Parco Area delle Scienze 37/A, 43124, Parma, Italy
[d] AIXTRON SE, Dornkaulstrasse 2, 52134, Herzogenrath, Germany

ARTICLE INFO

Keywords:
Multi-junction
MOVPE
SiGeSn
III-V
CPV

ABSTRACT

In order to produce a step forward towards the monolithic integration of III-V and IV compounds in multijunction solar cells, a first assessment of SiGeSn deposition in a metal organic vapour phase epitaxy (MOVPE) chamber also used for III-V growth has been carried out. The study brings insights on several aspects of the MOVPE SiGeSn growth in order to get a better control of SiGeSn composition and to obtain epitaxial layers with improved morphology. In particular, it is shown that the gas source Si_2H_6 is more influenced by the growth temperature compared to GeH_4 and $SnCl_4$, moreover, its competition with $SnCl_4$ makes it difficult to incorporate Si in SiGeSn, as $SnCl_4$ partial pressure is increased. SiGeSn morphology is shown to be strongly dependent on temperature, As carry-over and growth rate. A new growth model is introduced in order to explain the importance of the adatom bond lengths in inhibiting tin segregation when SiGeSn is grown at relatively high growth temperatures (>480 °C). In order to investigate the photovoltaic behaviour of SiGeSn, a single-junction GaAs/InGaP/SiGeSn/Ge functional device has been manufactured and characterized by external quantum efficiency (EQE) and current-voltage measurements. The experimental and the simulated EQE show the higher absorption coefficient of SiGeSn with respect to Ge, which allows using SiGeSn layers with a thickness three times lower than Ge to produce the same photovoltaic current.

1. Introduction

An effective solution to increase the photovoltaic (PV) conversion efficiency is the exploitation of multi-junction (MJ) solar cells technology. For this purpose, there is considerable interest for combining III-V and IV elements, exploiting the band gap engineering possibilities which this integration offers. SiGeSn, in particular, has been proposed to be used for thermophotovoltaic (TPV) applications and as a third junction in InGaP/InGaAs/SiGeSn/Ge devices, all lattice matched to Ge substrate [1–3]. The use of SiGeSn in multijunction (MJ) devices could allow replacing the metamorphic 1eV - InGaAs [4], which cannot be grown lattice matched to Ge, or the 1eV - InGaNAs, which showed low quantum efficiency when grown by Metal Organic Vapour Phase Epitaxy (MOVPE) [5].

However, the growth of defect free SiGeSn layers and the integration of SiGeSn in III-V structures has soon been recognized as not straightforward. Because of the high value of the lattice constant of tin as compared to that of Ge and Si, the solid solubility of tin in the SiGeSn alloy is very low, therefore, a phase separation either on the surface - with Sn segregation - or in the volume - with Sn precipitation - can take place. Phase diagram calculations [6] show that, at room temperature, tin concentration ≥1% can only be obtained by considering growth condition out of equilibrium and by applying kinetic barriers that do not allow reaching the equilibrium concentration. Literature results on binary GeSn, for example, evidenced that strain and the growth temperature play a central role in Sn incorporation [7]. In order to avoid Sn segregation/precipitation the growth temperature has been decreased to values below 350 °C [8,9]. This requirement has introduced two main challenges on (Si)GeSn deposition, namely: i) the necessity of identifying suitable gas precursors with low cracking temperature [10], and ii)

* Corresponding author. RSE, Strada Torre della Razza, le Mose, 29100, Piacenza, Italy.
E-mail address: gianluca.timo@rse-web.it (G. Timò).

https://doi.org/10.1016/j.solmat.2021.111016
Received 15 October 2020; Received in revised form 9 February 2021; Accepted 11 February 2021
Available online 24 February 2021

the ability to control the deposition in the kinetic regime, where small variations of temperature can cause gradient in the alloy composition and the low diffusivity of the atomic species on the surface can penalize the semiconductor crystallographic quality. In particular, the request of the low temperature deposition introduces a challenge in the in-situ growth control, since the pyrometers used for this purpose in most commercial MOVPE systems start working over 400 °C.

Eventually, the monolithic integration of SiGeSn in III-V based structures is hindered by the "*cross contamination*" problem: III-V elements are dopants for IV-based alloys and vice versa. The severe consequence of growing a sequence of III-V and IV based semiconductors in the same growth environment is the difficulty to control their conductivity, as shown, for example, by E. Welser et al., who measured memory effects of Ge in III-V alloys [11]. This explains why, so far, the integration of SiGeSn in III-V based MJ solar cells has been accomplished by using two pieces of equipment: a CVD reactor for the growth of the ternary SiGeSn and a MOVPE growth chamber for the deposition of the remaining III-V part of the cell structure [12,13]. Similarly, GaAsP/SiGe tandem structures have been realized by growing SiGe epilayers by reduced pressure chemical vapour deposition (RPCVD) and the III-V epilayers by MOVPE [14]. As a further example, the integration of Ge and III-V for the realization of heterojunction bipolar transistors has been carried out by using an ultrahigh vacuum (UHV) electron-beam evaporation system for the Ge deposition and a MOVPE system for the growth of GaInP [15].

The utilization of twofold growth equipment, however, introduces high capital expenditure and decreases the economic advantage of the monolithic architectures for the MJ photovoltaic application. As far as the authors' knowledge is concerned, only few attempts have been carried out on the growth of III-V and group IV elements in the same MOVPE growth environment. Preliminary experiments concerning the growth of epitaxial germanium in a MOVPE reactor utilized for III-V growth were carried out by R. Jakomin et al. [16]. G. Timò et al. showed the importance of modifying the MOVPE hardware to limit the cross-contamination of IV elements in III-V compounds [17] and then manufactured monolithic triple junction (TJ) InGaP/InGaAs/SiGe/Ge structures whose performances were slightly lower than those obtained on the standard InGaP/InGaAs/Ge TJ structure [18]. More recently, Ge single junction solar cells were grown by MOVPE with the in-situ growth of the InGaP window layer [19] along with the deposition of $(GaAs)_{1-x}(Ge_2)_x$ alloys [20].

The purpose of this contribution is to assess the potential of growing SiGeSn layers in a MOVPE growth chamber that is also used for III-V deposition, in order to produce a step forward towards the monolithic integration of III-V and IV compounds. In this first stage, diluted SiGeSn layers (i.e., layers with Si and Sn content <5%) have been deposited, searching for adequate growth conditions and suitable commercial gas precursors that can prevent tin precipitation/segregation in SiGeSn. At the same time, the growth temperature has been kept as high as possible to allow controlling the temperature profile over the wafer surface during the MOVPE growth. The assessment of these potentialities is indeed relevant in order to pursue an industrial scale up of the SiGeSn MOVPE growth process for manufacturing low cost, monolithic, high efficiency PV devices.

2. Material and methods

The growth of the SiGeSn layers has been carried out by means of a modified AIX 2800G4 MOVPE "planetary" reactor, which can host 2 × 4 inch and 6 × 6 inch wafers on the same susceptor and a *double gas foil rotation* (DGFR) system. An overview of the MOVPE system growth chamber is depicted in Fig. 1. The DGFR system can use a different mixture of N_2/H_2 gases which are injected in the center zone and in the edge zone underneath the graphite satellite where the wafer is set. This allows an in-situ control of the temperature profile across the wafer, with the possibility to change the wafer temperature in a few seconds, owing to the low thermal inertia of the graphite satellites. The MOVPE growth chamber has been equipped with: i) a multi wavelength optical reflectometer (905 nm, 633 nm and 405 nm) for the growth rate determination, ii) an emissivity corrected pyrometer for wafer temperature measurement and iii) a deflectometer for the wafer bowing measurements. In order to reduce the cross contamination effects, the following hardware modifications have been preliminarily accomplished on the MOVPE growth apparatus: i) use of a triple gas injector with the possibility to inject the IV elements precursors in the growth chamber in different positions from different gas lines, called *top hydride*, *bottom hydride* and *metalorganic* (MO) lines; ii) increase of the gas injector diameter, in order to enhance the precursor utilization efficiency; iii) insertion of a quartz plate in the center of the cylindrical graphite susceptor (which stays at a substantially lower temperature than the susceptor), in order to minimize the deposition at the chamber center zone upstream of the leading wafer edge; iv), optimization of thermal decoupling between the ceiling and the top reactor cooling plate, in order to reach ceiling temperature >190 °C, at deposition temperature around 460 °C, allowing to decrease the unwanted parasitic deposition on the ceiling due to condensation.

In order to pursue an industrial scale up of the growth process, only commercially available precursors have been selected, namely: IBuGe, GeH_4 (10% in H_2 or 10% in N_2), Si_2H_6 (1000 ppm in H_2 or 10% in H_2) and $SnCl_4$. IBuGe is a metalorganic source, with a suitable vapour pressure whose value is similar to that of TMGa and therefore, it should allow the deposition with a growth rate comparable with that obtained

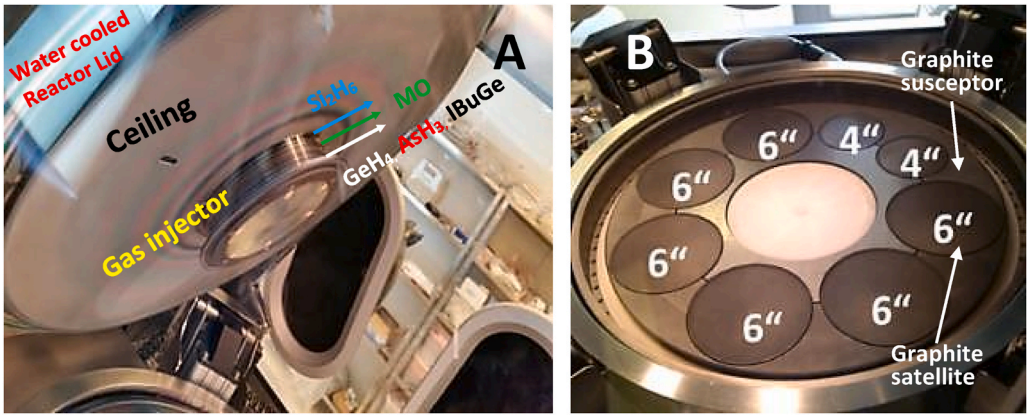

Fig. 1. Pictures of the inside of the AIX 2800G4 MOVPE "planetary" reactor: A) the graphite ceiling and the triple gas injector; B) the susceptor and the special wafer satellite pocket for an easier process transfer from 4 inch to 6 inch-. The areas of the ceiling and of the susceptor, which are sources of possible cross-contaminations, have been reduced with respect to the standard AIX 2800G4 configuration.

in III-V growth. Moreover it has been reported that IBuGe decomposes at 350 °C [21] with an activation energy of 27.4 kcal/mol [22]. GeH_4 is an alternative source to IBuGe, as it presents comparable activation energy [9]. Si_2H_6 is a commercially available gas, which has been already successfully used for SiGe growth at low temperature [23,24]. Eventually, with respect to SnD_4, utilized in the earlier experiments on SiGeSn [25], $SnCl_4$ is cheaper and easier to purchase. This source has also been selected because it was successfully used for GeSn growth [26]. As described in section 3.1 and 3.2.4, the growth of SiGeSn has also been carried out by adding AsH_3 and/or DEZn to the group IV sources. All MOVPE runs have been performed in the temperature range 450–500 °C, with a total gas flow rate between 12 and 18 l/min and using N_2 as carrier gas, which allows obtaining higher growth rate with respect to H_2 [27]. The reactor pressure has been kept fixed at 50 mbar. The SiGeSn layers have been deposited over 4 inch and 6 inch Ge substrates, with orientation (100) 6° off towards <111> and over 4 inch GaAs substrates with orientation (100), 2° off towards <110>. In order to change the level of As carry-over in the MOVPE growth chamber, between the SiGeSn under investigation and the last III-V growth, a different number of coating runs of group IV elements has been interposed, as indicated later. The epitaxial layers have been characterized by High Resolution X-Ray Diffraction (HRXRD), Scanning Electron Microscope (SEM) and Transmission Electron Microscopy (TEM) techniques, including Selected Area Electron Diffraction (SAED), High Angle Annular Dark Field Scanning Transmission Electron Microscopy (HAADF-STEM) and High Energy Dispersive X-ray mapping (EDX), Atomic Force Microscope (AFM), Secondary Ion-Mass Spectroscopy (SIMS) and Ellipsometry. The layer growth rate has been evaluated by fitting the MOVPE in-situ reflectance curves or by SEM analysis in cross-section. By considering that SiGeSn layers with the same lattice constant can be obtained with different pairs of Si and Sn concentrations [28], the SiGeSn composition has been determined by combining HRXRD and SIMS characterization (see Supplementary Information). Quantum efficiency (EQE) and current–voltage (IV) measurements have been eventually carried out to characterize a GaAs/InGaP/SiGeSn/Ge single junction functional device. The list of the grown SiGeSn samples is reported in Table 1.

3. Results and discussion

3.1. Preliminary MOVPE growth of SiGeSn by IBuGe, Si_2H_6 and $SnCl_4$

Preliminary experiments have been carried out by depositing SiGeSn layers, with Ge concentration around 98%, with the use of IBuGe, Si_2H_6 (1000 ppm in H_2) and $SnCl_4$ precursors. A small arsine overpressure (P_{AsH3} = 4 Pa) was introduced in the growth chamber in order to improve the surface morphology, as already reported for the growth of pure epitaxial germanium samples by IBuGe [29]. These first SiGeSn runs were carried out only after six MOVPE SiGe(Sn) coating runs from the last III-V deposition. SiGeSn HRXRD characterization of samples grown with different thickness and with the same gas phase composition is shown in Fig. 2. The SiGeSn diffraction peak position is almost unvaried in the center of the wafer, indicating no change in the average lattice parameter with different thickness. By acquiring a series of HRXRD ω−2θ scans along the wafer radius, a shift of the SiGeSn peak towards larger 2θ angles is noticed. Since the concentrations of Sn and Si in SiGeSn have opposite effects on the lattice parameter (i.e., Sn increases, while Si decreases the lattice constant value), the results reported in Fig. 2b could be explained both by a decrease of Sn and/or an increase of Si incorporation in the ternary layer going from the center to the wafer edge. By fitting the in-situ reflectance measurements of the SiGeSn layers grown on the GaAs substrate, a growth rate of 3 nm/min has been calculated. SIMS measurements, reported in Fig. 3, allow calculating a distribution coefficient of Si (i.e., the ratio between the Si content in the solid and the value of the Si_2H_6 gas phase composition) around 0.04. A concentration of Sn <0.5% was determined by HRXRD measurements.

The morphology and microstructure have been analysed by top view SEM and cross section TEM (Fig. 4). The SEM image reported in Fig. 4a allows the classification of two main different morphological defects in SiGeSn samples grown on Ge: i) A-type round-shaped defects, about 250 nm in size, with a homogenous structure and ii) B-type round-shaped defects, about 1.5 μm in diameter, including an agglomerate of nanocrystals. The cross section HAADF-STEM images of A- and B-types of defects are shown in Fig. 4b and e, respectively. A-type defects consist of SiGeSn protrusions with some structural extended defects at the edges (Fig. 4b and c). The SAED pattern in the inset of Fig. 4b shows that the bumps are monocrystalline and epitaxially grown on the substrates. The chemical composition is homogeneous across the A-type defects, as shown in the EDX map in Fig. 4d. On the other hand, B-type defects consist of columnar grains with dimensions of some tens of nm (Fig. 4e). The corresponding ring SAED pattern (inset), reveals that the nanocrystals are randomly oriented. In addition, bright regions at the base of the nanocrystals are observed in the HAADF-STEM images (Fig. 4f), suggesting higher-Z element segregation. The EDX map analysis confirmed the presence of Sn-rich regions at the base of B-type defects, as shown in Fig. 4g. We can therefore conclude that tin precipitates during the deposition and probably causes the loss of the epitaxy. Owing to the relatively high deposition temperature (460 °C), tin precipitation could be expected, however, as shown later, we obtained tin precipitation free SiGeSn layers even at higher temperature. The origin of tin precipitation will be clarified in the next paragraphs.

Table 1
Growth rate and composition results on MOVPE SiGeSn deposition in a III-V contaminated reactor.

MOCVD runs	T_{growth} (°C)	$P_{par\ IBuGe/GeH4}$ (Pa)	Zn dopant	$SnCl_4$ gas phase comp. (%)	Si_2H_6 gas phase comp. (%)	GR (nm/min)	Si from SIMS (%)	Sn XRD sim. (%)	Notes
S1and S2	460	71 ([a])	No	1.5	8.8	3	0.5	<0.5	**AsH_3 during deposition**
S3–B	475	37.8	No	3	13.7	-	-	-	**Rough morphology**
S3-A	486	37.8	No	3	13.7	5	<2	-	**6 inch**
S4-A	486	37.8	No	2.9	13.7	-	1.6	0.5–0.6	**6 inch**
S4–B	490	37.8	No	2.9	13.7	5.2	-	-	–
S5–B	489	37.8	Yes	3	13.7	7.4	2	0.6	**Thickness 665 nm**
S5-A	491	37.8	Yes	3	13.7	7.4	3	0.7	**6 inch**
S6	487	37.8	Yes	3	13.7	-	-	-	–
S7–B	490	39	Yes	7.7	36.7	13.4	3	0.9	**Thickness 1610 nm**
S7-A	500	39	Yes	7.7	36.7	-	-	-	**Sn precipitation, 6 inch**
S8	487	37.8	Yes	3	13.7	-	-	-	**Sn precipitation, deposition in clean growth chamber**
S9	487	37.8	Yes	3	13.7	-	-	-	**After GaAs/Ge coating**
S10	**480**	**37.5**	**Yes**	**7.7**	**36.7**	**5.5**	**2**	**0.55**	**N_2 Diluting gas in GeH_4**

[a] The value refers to the IBuGe partial pressure. All runs are on 4 inch wafers, if not otherwise stated in the notes.

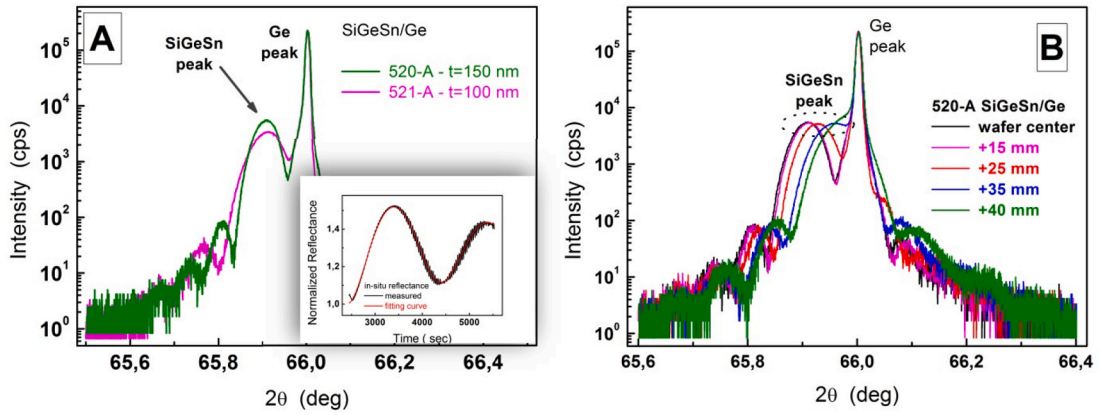

Fig. 2. A) HRXRD ω−2θ curves acquired in correspondence of (004) symmetric reflection, at the center of the wafers, related to SiGeSn samples grown with different thickness, with the following gas partial pressure: $P_{IbuGe} = 71$ Pa, $P_{SnCl4} = 1.2$ Pa, $P_{Si2H6} = 7$ Pa. In the inset, the fitting of the in-situ SiGeSn reflectance measurement over GaAs substrate. B) characterization of the SiGeSn composition uniformity on sample S1.

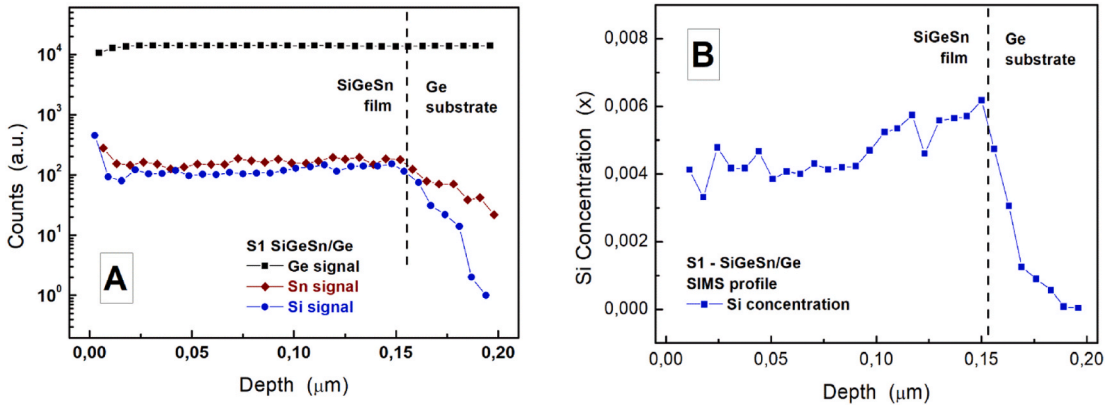

Fig. 3. SIMS profiles as measured on the SiGeSn/Ge (S1) sample: A) comparison between the raw data, B) Si concentration determination, using the SiGe standards.

3.2. MOVPE growth of SiGeSn by GeH_4 (10% diluted in H_2 or N_2), Si_2H_6, (10% diluted in H_2 or Ar) and $SnCl_4$

IBuGe has then been replaced with GeH_4, 10% diluted in H_2 or N_2, and the concentration of Si_2H_6 in H_2 has been increased from 1000 ppm to 10%. In this SiGeSn growth series, arsine was not used during the deposition. The deposition series starts from sample S3, which took place after forty MOVPE coating runs of (Ge)Si from the last III-V run. Therefore the MOVPE reactor was less contaminated by As with respect to the previous, S1 and S2 SiGeSn samples. From run S3 to run S7 only SiGeSn depositions have been performed. The S8 run was carried out in a clean reactor without As carry-over. The S10 run was performed after eight Ge coating runs from the last III-V deposition. Then for this last run, the reactor chamber presented an As carry-over comparable with the carry-over that was present in the growth of sample S1 and S2.

3.2.1. Crystal quality and composition uniformity

The crystal quality of SiGeSn lattice matched on Ge has been investigated both on 4 and 6 inch wafers. In general, in the center of the samples, HRXRD analysis shows intense interference fringes around the main peak. On the edge of the samples, interference fringes are not observed, showing the presence of stronger compositional gradient at the interface between SiGeSn and Ge substrate. By analysing the HRXRD peaks separation, on 4 inch wafers, a composition non-uniformity lower than 1% has been estimated, this value increases to around 3% on 6 inch wafers, as also shown by SIMS results (see Fig. 5).

Since the deposition on 4 and 6 inch wafers took place in the same MOVPE run, the different uniformity obtained on the two wafers is a limitation imposed by the kinetic growth regime: the gas sources change their residence time as long as they proceed horizontally over the wafer surface, therefore the efficiency of the chemical reaction cannot be uniform along the wafer radius, producing a variation of the thickness and of the layer composition. In principle, a better uniformity can also be obtained on 6 inch wafers by modifying the growth parameters that were optimized for the growth over 4 inch wafers. In particular, in the kinetic regime, a proper temperature gradient imposed over the wafer should help in improving the deposition uniformity. For this purpose, the MOVPE reactor was set up with a special design of the gas foil rotation, which allowed changing underneath the wafer, in the center and at the edge, the mixture of hydrogen and nitrogen. Unfortunately at the low temperature necessary for the SiGe(Sn) growth, the use of hydrogen in the gas foil rotation has a drawback: as in the case of Si, it passivates the Ge surface and blocks the growth [30,31], therefore the growth rate at the wafer edge is strongly reduced. In this case, the use of the special design of the gas foil rotation brings an advantage in the modulation of the temperature over the wafer radius. However, at the same time, a certain reduction of the wafer yield, owing to the reduction of the growth rate at the wafer edge, has to be expected. Alternatively, in order to improve the deposition uniformity on 6 inch wafers, the total gas flow can be increased, by accepting a reduction in the precursors utilization efficiency.

An excellent crystal quality has been found in the sample S3-A (deposited on a 6 inch wafer) and in the sample S4–B (deposited on a 4 inch wafer), whose HRXRD characterization is shown in Fig. 6a. The S3-A, grown at lower temperature, is slightly shifted on the left side of the S4–B peak, which is overlapped to the Ge one. Remarkably, the low

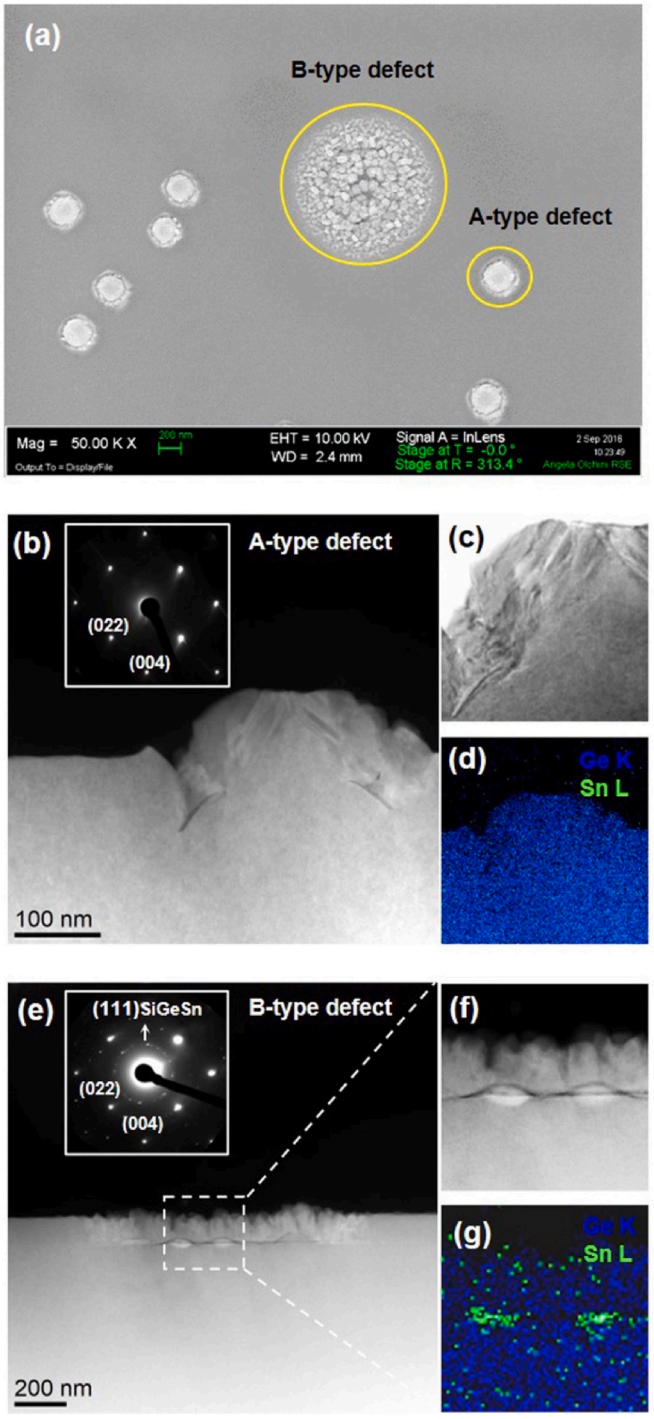

Fig. 4. a) Top view SEM image of sample SiGeSn/Ge S1; b, c, d) cross section TEM analysis of an A-type defect: b) HAADF-STEM image with the corresponding SAED pattern in the inset, c) conventional TEM image of the left edge, d) EDX map; e f, g) cross section TEM analysis of a B-type defect: e) HAADF-STEM image with the corresponding SAED pattern in the inset, f) high-magnification of the region marked in (e), g) EDX map.

FWHM of the diffraction peaks (48 arcsec) along with the high sensitivity of the X-ray based technique allow us clearly distinguishing the epilayer peak from the substrate one, in spite of their low lattice constant difference of 0.035%. The sample S10, grown with GeH_4 diluted in N_2, also shown a comparable crystal quality clearly evidenced by the high contrast interference fringes in the ω−2ω curve (see Fig. 6b).

The lattice-matched samples have been used to assess the method applied to get the Sn concentration in diluted SiGeSn alloys, by using as input the Si incorporation measured by SIMS and then fitting the XRD peak. The results have been compared with literature data [6,32] (see Supplementary Information).

3.2.2. SiGeSn composition control

If we compare the HRXRD measurements reported in Figs. 2b and 5a, we may infer that the increment of the deposition temperature from run S1–S2 to run S5–B could have favoured a better composition uniformity along the wafer radius. As already observed, the shift of the HRXRD peak to higher 2θ angle, that indicates a smaller lattice constant, could be due in principle to a higher Si concentration or/and to a lower Sn concentration in SiGeSn, as Si (Sn) incorporation have been reported to increase (decrease) by increasing the growth temperature [33]. However, since Si incorporation exponentially increases with the growth temperature, with an activation energy higher than Sn [34], we could conclude that the distribution of silicon is the main responsible of the worse composition uniformity found on sample S1–S2 and also on sample S5-A, the last one, carried out on 6 inch wafer. This hypothesis has been confirmed by SIMS measurements as reported in Fig. 5c. It is worthwhile to point out that the temperature difference between the center and the edge of the sample S5-A was just 2 °C, with the edge being at higher temperature. In the kinetic regime, the role of temperature is thus of primary importance concerning the Si_2H_6 decomposition and the related Si incorporation in SiGeSn. This is also shown, in particular, by the variation of the Si distribution coefficient with the growth temperature, which increases from 0.04 to 0.11 and then to 0.14, from the run S1–S2 to run S4-A and then to run S5–B, grown at 460 °C, 486 °C and 489 °C, respectively.

Si distribution coefficient drops from 0.14 in run S5–B to 0.08 in the run S7–B, despite both MOVPE runs have been carried out at almost the same temperature (489 °C and 490 °C, respectively), probably due to the stronger competition between Si_2H_6 and $SnCl_4$. In fact, in run S7–B the quantities of both precursors have been increased with respect to run S5–B. It results that, the higher the $SnCl_4$ gas phase composition, the more difficult it is to incorporate Si in the SiGeSn layer. The competition between Si_2H_6 and $SnCl_4$ becomes more evident by comparing the growth of SiGe and SiGeSn. We grew SiGe at 475 °C (not here reported) with a Si_2H_6 gas phase composition of 6% getting around 3.5% of Si in the solid (with a Si distribution coefficient reaching 0.58). These values have to be compared with those obtained in run S5–B, grown even at 489 °C: with a Si_2H_6 gas phase composition of 13.7% and $SnCl_4$ partial pressure of 5 Pa, the silicon incorporated into the solid was only 2% (see Table 1). The competition between Si_2H_6 and $SnCl_4$ along with the kinetic growth regime introduce a loss of linearity between the gas phase and the solid composition, which can be inferred by comparing again runs S5–B and S7–B. Between the two runs, the Si_2H_6 and $SnCl_4$ gas phase compositions have been both increased by a factor approximatively equal to 2.6, however, the Si and Sn solid composition have increased only of 50% (Si increased from 2% to 3% and tin from 0.6% to 0.9%).

3.2.3. SiGeSn surface morphology

The surface morphology of SiGeSn grown in a III-V contaminated growth chamber has been observed to be strongly temperature dependent, as well as influenced by the level of As carry-over in the growth chamber and by the growth rate (see Fig. 7). At temperatures around 475 °C, the SiGeSn surface becomes rough, while at temperature around 500 °C, strong Sn segregation appears. Morphology can improve at temperature lower than 475 °C, as in the case of S1, grown at 460 °C, if AsH_3 is injected in the growth chamber during the run, showing the role of As in preventing the morphology deterioration, as better described later. A more in depth morphology analysis carried out by AFM shows that SiGeSn layers grown in the temperature window 480 °C–490 °C present defects, at different concentration and size, which look like etch pits, correlated with the Sn content in the samples. The presence of holes

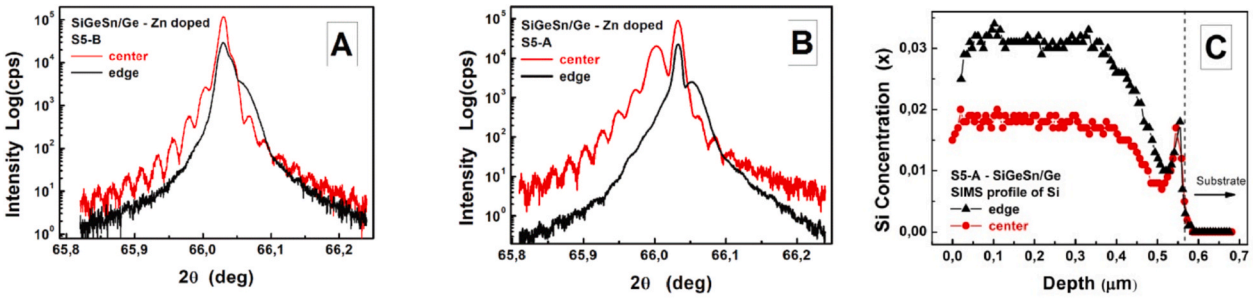

Fig. 5. HRXRD ω−2θ curves measured at the center and at the edge of: A) the 4 inch wafer S5–B, B) the 6 inch wafer S5-A; C) Silicon concentration measured by SIMS at the center and at the edge of the 6 inch wafer (S5-A). The samples have been grown with Si_2H_6 and $SnCl_4$ partial pressure of 6.25 Pa and 1.3 Pa, respectively. The spikes at the SiGeSn/Ge interface are due to a measurement artifacts.

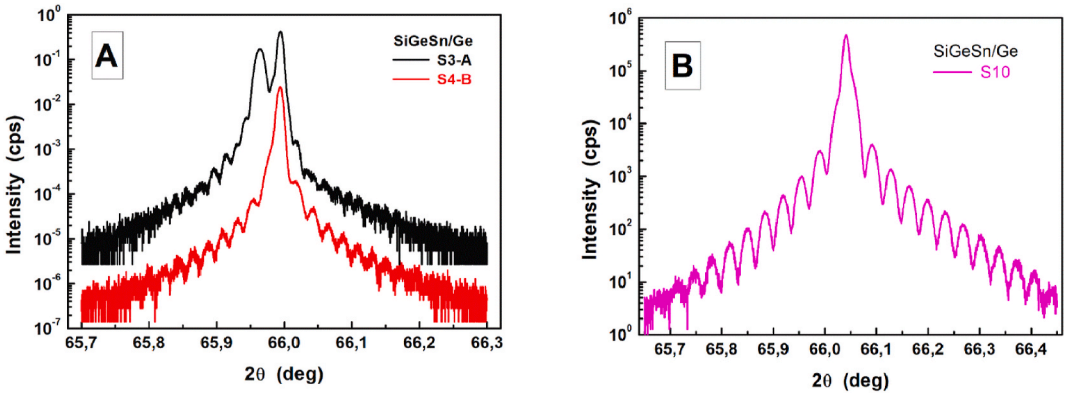

Fig. 6. HRXRD ω−2θ curves on SiGeSn/Ge samples; A) comparison between sample S3-A and S4–B (grown at temperature 4 °C above S3-A). The intensity of the S4–B ω−2θ curve has been down shifted in order to favour curve comparison; B) ω−2θ curve of S10, showing high contrast interference fringes, demonstrating excellent crystal quality.

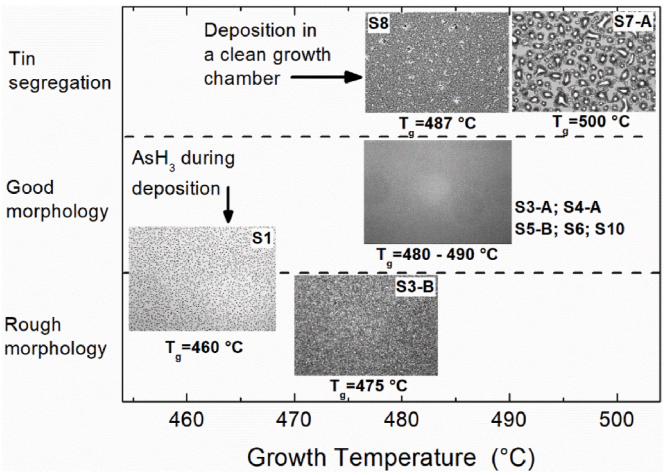

Fig. 7. Morphology diagram for the SiGeSn growth with GeH_4 or IBuGe precursors in a III-V contaminated reactor, if not otherwise stated. Images taken at optical microscope with 500x magnification.

on the SiGeSn surface was also observed by Lupien at al. [35] and it was attributed to bulk diffusion of Sn and its evaporation from the surface. Etch pit defects have also been observed on SiGe owing to Ge evaporation from the surface [36]. Since, in our samples, SIMS characterization showed almost constant Sn concentration along the thickness (see Fig. 8), we suppose that Sn could evaporate from the SiGeSn surface during the cooling phase of the MOVPE growth run. A sample with a higher Sn content should therefore present a more pronounced evaporation phenomenon and an increase in the "porosity" of the surface. This behaviour is shown by AFM images of samples S5–B and S7–B reported in Fig. 8. TEM cross section analysis carried out on sample S7–B evidences a defect free and sharp interface between Ge and SiGeSn and that the pores are indeed confined on the surface, presenting different size, especially along the growth axes (see Fig. 9). If pores are due to Sn evaporation, their different dimensions could be considered a sort of footprint of a locally-varying Sn incorporation. Further experiments are under investigation in order to confirm whether the SiGeSn surface degradation takes place at the end of the MOVPE run, by covering the SiGeSn with thin SiGe/Ge cap layers before starting the cooling stage.

3.2.4. A theory on the role of the bond length of adatoms in inhibiting tin segregation

Most of the published results on SiGeSn deposition stress the importance of decreasing the growth temperature to values lower than 350 °C in order to avoid Sn precipitation or segregation (see, for example [25,28,37]). Recently a detailed analysis of the influence of SiGeSn morphology as a function of temperature has been reported by R. Khazaka et al. [34]. However, one important finding of our experiments is the possibility to get SiGeSn tin-precipitation free even at temperatures around 490 °C. We have assessed that this possibility is linked to the presence of As in the growth chamber, owing to the previous III-V runs. We have indirectly ascertained the presence of As in the growth chamber, by measuring the incorporated As in the SiGeSn samples by SIMS as shown in Fig. 10. The inhibiting role of As for tin precipitation/segregation was already reported by Nupur Bhargava et al., who introduced AsH_3 during SiGeSn runs [38]. Without entering in a detailed explanation, the authors considered the role of As as a surfactant which can suppress the islanding and/or Sn segregation. If we consider that the driving force for segregation is the energy gain obtained when Sn

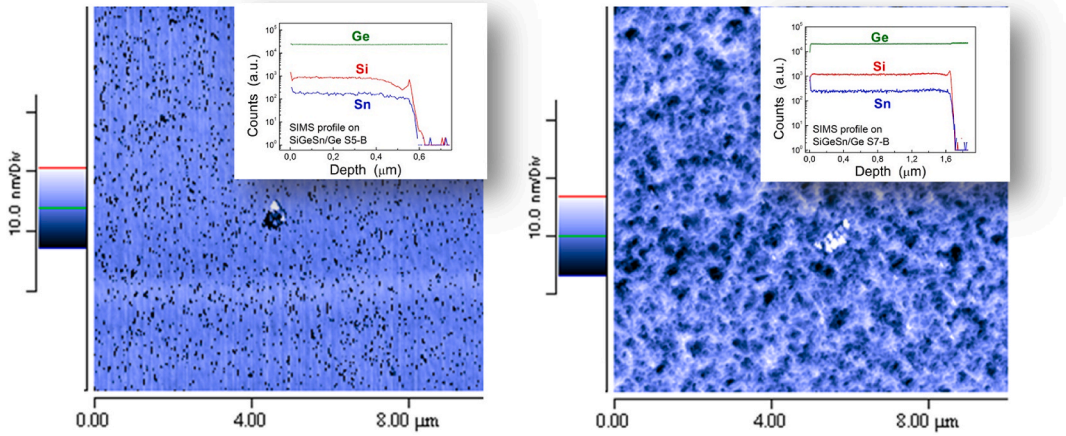

Fig. 8. AFM images of sample S5–B (left) containing 0.6% of Sn and S7–B (right) containing 0.9% of Sn. In the insets the corresponding SIMS profiles of the Ge, Si and Sn elements.

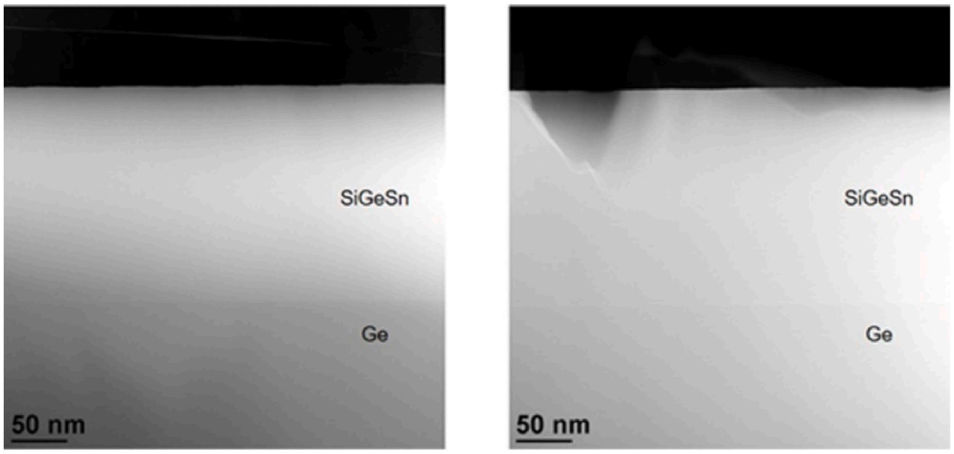

Fig. 9. Cross section HAADF-STEM images of sample S7–B taken at different regions. The image on the right shows differently sized holes at the surface, as evidenced by AFM in Fig. 8.

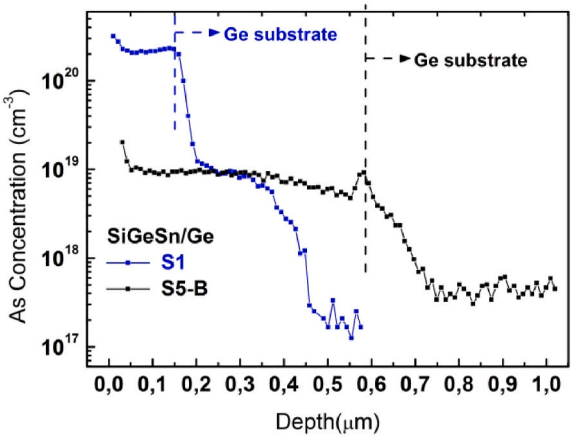

Fig. 10. Comparison between SIMS profile of As in SiGeSn samples S1 and S5–B, deposited in a MOVPE growth chamber with a different As carry-over.

incorporated in the crystal exchanges its position with a Ge adatom on the surface, we can also argue that the presence of As adatoms on the surface could disfavour this process. By considering that the bond length increases from Ge–Ge (242 pm) to Ge–As (247 pm), the exchange process would then be inhibited, because the compressive strain value reached with Sn segregated on the surface with As adatoms could be higher than that generated with Sn incorporated in the SiGeSn crystal. Kasper showed that, for low Sn adatom coverage, the Sn surface adatom concentration, C^s_{Sn}, is linearly linked to the Sn bulk concentration C^b_{Sn}, through the segregation length, Δ_s [39]:

$$C^s_{Sn} = \Delta_s C^b_{Sn}$$

Therefore, we could assume that the presence of As adatoms is equivalent to a decrease of the segregation length. Since this length is strongly temperature-dependent, and in particular, it decreases by decreasing the temperature (see again [39]), we can conclude that the presence of As adatoms on the Ge surface has the same effect of decreasing the growth temperature. This explains why it is possible to grow SiGeSn layer Sn segregation free even at temperatures up to 490 °C. If the bong length of adatoms determines the inhibiting role for Sn precipitation, we would expect that the use of phosphine (PH_3) would not be as effective as AsH_3, since the bond length of Ge–P is 230 pm. As a matter of fact, we used PH_3 during a SiGeSn growth and we did observe Sn segregation. According to this theory, the use of Sb-based precursors could be more effective than AsH_3, since the Ge–Sb bond length is higher (266 pm) than the Ge–As bond length. However, since both As and Sb give n-type polarity to SiGeSn, other precursors have to be searched to get p-type SiGeSn tin precipitation free. A possible solution could be the use of cyclopentadienylmagnesium (Cp_2Mg), $(C_5H_5)_2Mg$, since Mg is a

group II element and the bond length of Ge–Mg is 271.9 pm [40]. It is worth noting that also Zn could be a p-type dopant for Ge, however, the Zn–Ge bond length is 238.38 pm and again we assessed that the use of DEZn cannot be effective in inhibiting Sn precipitation. On the other hand, we have observed that the use of DEZn helps increasing the growth rate, as shown by comparing the growth rate measured on samples S4–B and S5-A. While other possible pathways to suppress Sn segregation can be considered to explain the experimental results, like, for example, the interaction between the adsorbed As with Sn precursor, the proposed surface-driven mechanism, if confirmed by the test with $(C_5H_5)_2Mg$, will allow addressing the considerable achievement of producing both p-type and n-type SiGeSn at relatively high temperature.

It could be speculated that the absence of Sn segregation could be due to the low Sn incorporation in our samples, as Sn concentration lower than Sn solid solubility has been measured by SIMS. However, this hypothesis is contradicted by the fact that when SiGeSn samples are grown around 490 °C, adopting very similar growth parameters (i.e. input precursor partial pressure and temperature), but without As adatoms, Sn segregation takes place.

We proved this concept by growing SiGeSn in a clean growth chamber (run S8), that is, with susceptor, satellites and ceiling that did not see any deposition and then by repeating the SiGeSn deposition (run S9), after a Ge/GaAs coating run. GaAs was deposited to make available in the growth chamber a source of As atoms, Ge deposition over GaAs was carried out in order to reduce/control As in the growth environment. The drastic variation of morphologies of runs S8 and S9 and the segregation of Sn only in the sample S8, as shown in Fig. 11, indicate that an accurate control of the As in the MOVPE growth camber is indeed of paramount importance to avoid Sn segregation at the considered deposition temperature. It is worthwhile to point out that since both S8 and S9 samples have been grown in the temperature window where it is possible to obtain, as shown in Fig. 7, SiGeSn Sn segregation free and by using very similar precursor partial pressure, we can rule out any temperature or growth rate dependence on Sn segregation. Furthermore, in our research we presented results on lattice matched samples, therefore the role of dislocation in the Sn incorporation and segregation can also be disregarded.

From this point of view, it is not surprising that the quality of the grown layers could suffers of some structural defects, despite they show compositions around the expected equilibrium content, because the morphology deterioration has not been ascribed to an excess of Sn with respect to the equilibrium value but it has been related to the growth mechanism which develops at the beginning of deposition.

3.2.5. *Role of the growth rate on tin precipitation*

N. Taoka et al. found significant Sn migration and desorption in 200 nm thick SiGeSn samples grown at 350 °C, with a Sn concentration which doubled during the growth process; they concluded that the amount of segregated atoms increases by increasing the thickness [41]. From run S3–B to run S7–B, carried out in the temperature range 475 °C–490 °C, we have not observed Sn migration during the SiGeSn growth, in spite our SiGeSn samples are much thicker than the samples considered in Ref. [41] and are grown with a temperature 140 °C higher. As shown by SIMS analysis reported in Fig. 8, we can point out only a small increase in the Sn concentration in the first 200 nm of SiGeSn deposition, followed by a stable Sn concentration all over the run duration; moreover we have not observed any increase of Sn migration by growing thicker samples, in particular passing from run S5–B, 665 nm thick, to run S7–B, 1.61 μm thick. A possible explanation for the encountered differences could be found by considering the higher growth rate and the lower Sn concentration utilized to deposit our samples: 7.4 nm/min for the run S5–B and 13.4 nm/min for the run S7–B vs 1.6 nm/min utilized by N. Taoka et al., while Sn was around 1% in our samples vs 4.5% in their samples. Of course, the Sn segregation process becomes more and more important as much as we overcome the Sn equilibrium concentration allowed in SiGeSn. However, also J. Margetis et al. reported a quite homogenous Sn distribution throughout the epilayer of GeSn samples even with 7% of Sn in the alloy, deposited at temperature <450 °C with a growth rate higher than 20 nm/min [26]. Therefore, we are induced to conclude that the growth rate is a key parameter to contrast Sn migration and this could explain why in spite of the utilization of arsine during the growth, we observe tin precipitation in run S1, which was carried out at 460 °C but with a growth rate much lower than the sample S5–B (3 nm/min, vs 7.4 nm/min, respectively).

3.2.6. *Characterization and simulation of a GaAs/InGaP/SiGeSn/Ge single junction solar cell*

The complex dielectric function of sample S5–B has been determined by Ellipsometry and compared to the Germanium one; the best-fit procedure to the experimental spectra with the semiconductor parametric model by WVASE® software gives refractive index and absorption coefficient spectra of Fig. 12a. The overall SiGeSn spectra have a similar critical point (CP) structure with respect to Ge, with increased CP broadening and a slight blue shift of the E_0 direct bandgap (0.86 eV vs 0.79 eV). An indirect absorption edge should be extrapolated at about 0.62 eV (E_g); likely owing to the high As incorporation, the absorption coefficient of the SiGeSn sample presents a broad Urbach band tail, and the absorption becomes higher than for Ge below the direct bandgap. For comparison D. Phoebe-Pearce et al. [42] reported E_0 at 0.87 eV for SiGeSn film with similar composition (3% Si, 0.8% Sn); calculations from linear interpolation formulas [43] for the present composition (2% Si, 0.6% Sn) give 0.83 eV–0.68 eV bandgaps at Γ and L valleys, respectively. The low bandgap of SiGeSn is due to the diluted nature of SiGeSn layers. In order to get higher bandgap and make the material suitable to be used as a third junction in a four-junction solar cell, an increase of Sn and Si incorporation will have to be accomplished.

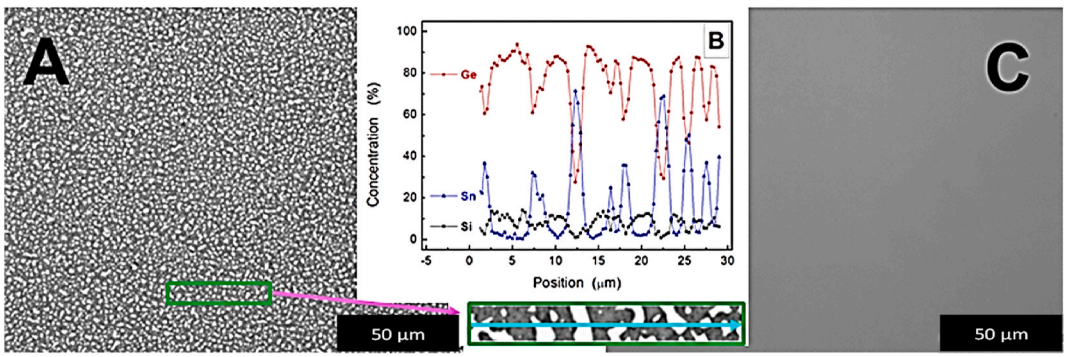

Fig. 11. Optical microscopy images of the morphology of SiGeSn deposited in A) a growth chamber with a clean susceptor and satellites (run S8); C) after GaAs and Ge coating on the susceptor and satellites (run S9). For both MOVPE runs the same gas phase composition has been utilized; B) EDX line scan to assess Sn segregation, carried out on the region of the sample S8 depicted by the SEM image. Sn segregation is absent on sample S9.

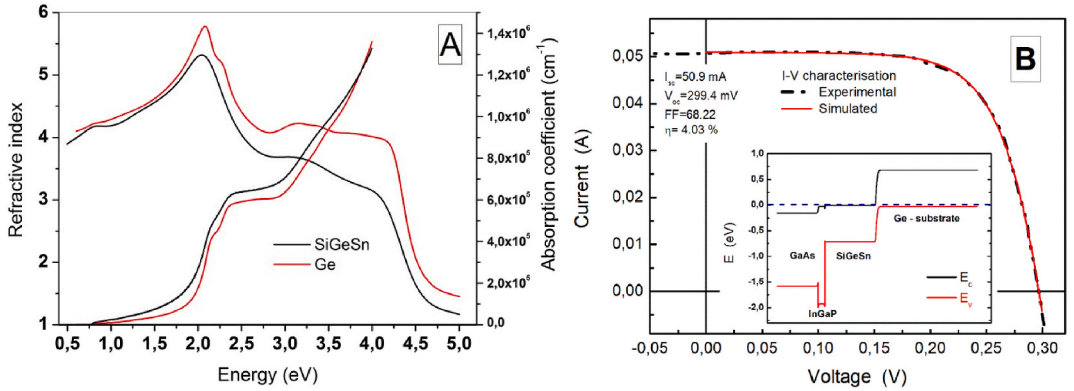

Fig. 12. A) Absorption coefficient and refractive index spectra of SiGeSn sample S5–B and bulk Ge. B) IV curve obtained under AM1.5D spectrum with 50x concentration of the GaAs/InGaP/SiGeSn/Ge single junction; in the inset the energy band diagram (thicknesses not in scale) of the heterojunction. Solar cell designated area = 0.0538 cm^2, with mask shadowing (front metal area/total cell area of 26%).

The higher absorption coefficient of SiGeSn with respect to Ge has also been confirmed by measuring and simulating the IV characteristic and the EQE of a GaAs(n-type)/InGaP(n-type)/SiGeSn(n-tpe)/Ge(p-type) heterojunction (see Figs. 12b and 13a), whose SiGeSn layer, 0.6 μm thick, has been grown in the same condition of sample S5–B. A GaAs layer, 0.4 μm thick, has been grown on top of the structure in order to improve the ohmic contact. In order to simplify the manufacturing process, this cap layer has not been removed from the front side of the device, so it also behaves like a light filter. The InGaP layer, 0.065μm thick, has been used in the attempt to passivate the SiGeSn emitter. The cell structure has been finally coated with a SiO_2/Ta_2O_5 stack. For the front and back contacts, Ti/Au/Ag/Au and Zn/Au/Ag/Au have been deposited with a total thickness of 4 μm and 2 μm, respectively.

The IV curve has been successfully simulated by using the EQE data and a triple diode model, whose pre-exponential terms, for the diffusion (J_0), recombination (J_{rec}) and tunnelling (J_{tun}) current density, along with the series (R_s) and shunt (R_{sh}) resistance assumed, respectively, the following values: $J_0 = 6.7 \times 10^{-6}$ A/cm^2, $J_{rec} = 1.53 \times 10^{-7}$A/$cm^2$, $J_{tun} = 2.5 \times 10^{-5}$A/$cm^2$, $R_s = 0.15$ Ω and $R_{sh} = 1100$ Ω. The short circuit current density (J_{sc} = 19.5 mA/cm^2 at 1 sun) is mainly limited by the high value of the surface recombination velocity between SiGeSn and InGaP, which from EQE simulation resulted to be $> 10^5$ cm/s. The open circuit voltage (V_{oc}) is limited by the low bandgap of SiGeSn. In order to bring the SiGeSn cell closer to a realistic condition in which SiGeSn behaves like a bottom cell in InGaP/GaAs/SiGeSn MJ structure, we cut the measured EQE, as reported in Fig. 13a, for all the wavelength <970 nm and we calculated the short circuit current density and then difference $W_{oc} = E_g/q - V_{oc}$ (see Supplementary Information). The calculated W_{oc} is 0.432 V. This value is quite similar to the value presented by Ge, as we could expect for dilute SiGeSn, and remarkable lower than the value that can be calculated from Ref. [44] (0.72 V), related to 1eV SiGeSn single junction.

For the simulation of the EQE, the scattering matrix method and a simplified solution of the continuity equation have been applied [45]. According to the band energy diagram (see the inset of Fig. 12b) only the SiGeSn emitter and the Ge base have been considered as active PV layers. In fact, the minority carriers generated in GaAs are blocked by the InGaP barrier, while carrier generation in InGaP is negligible owing to GaAs absorption. The simulated EQE data are in good agreement with the experimental ones, if we consider the following approximations: i) for the optical properties of InGaP and GaAs layers, literature data have been used, ii) in the reflectance modelling, the surface and interfaces have been considered optically flat, while the cell surface was somewhat rough and light scattering was produced. Fig. 13a shows that the main contribution to the short circuit current is given by the SiGeSn emitter. We have also simulated the EQE of a PV structure in which the SiGeSn has been replaced by a Ge emitter, by keeping the emitter thickness unchanged (see Fig. 13b). By comparing Fig. 13a with Fig. 13b, it is evident that a lower absorption takes place in the emitter when Ge is used instead of SiGeSn: the emitter contribution to the short circuit current reaches 72% when SiGeSn is used, while it drops to 47%, when Ge replaces SiGeSn.

It is interesting to point out that simulating the Ge emitter case, an EQE with a max around 0.8, instead of 0.7, has been obtained. This is due to the combined effects of a reduced absorption in the emitter and of a high recombination velocity at the interface between the emitter and

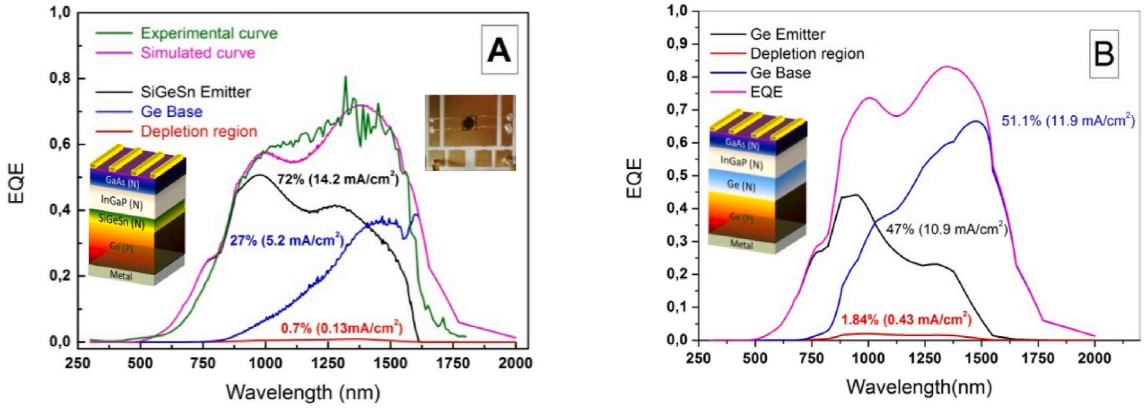

Fig. 13. A) Comparison between simulated an experimental data related to the GaAs(n-type)/InGaP(n-type)/SiGeSn(n-type)/Ge(p-type) single junction, B) EQE simulation of a GaAs(n-type)/InGaP(n-type)/Ge(n-type)/Ge(p-type) PV structure, with a Ge (n-type) layer with the same thickness of the SiGeSn emitter.

the InGaP. By replacing SiGeSn with Ge, while keeping the same value for the surface recombination velocity, we can generate more carriers in the base, where we have less non-radiative recombination, and consequently we can get higher EQE values. The higher absorption coefficient of SiGeSn with respect to Ge could be fully exploited once the recombination velocity at the interface SiGeSn/InGaP could be reduced, for example, to 10^2 cm/s. In this case, the contribution of the emitter to the short circuit current is expected to rise to 82.9% and the cell efficiency would be boosted from 4% to 7%. It is worthwhile to point out that, by keeping unchanged the surface recombination velocity at 10^2 cm/s and by using a Ge homojunction instead of a SiGeSn/Ge heterojunction, the EQE simulation shows that a Ge emitter thickness three times higher than a SiGeSn one would be required in order to get the same emitter contribution in the short circuit current. For TPV applications, where a high absorption in the infrared spectrum region is required, the reported experimental results on SiGeSn absorption coefficient along with the EQE simulations show that dilute SiGeSn based devices could conveniently replace Ge ones leading to higher EQE and conversion efficiency.

4. Conclusions

In this study, a first assessment of SiGeSn deposition in a MOVPE chamber also used for III-V growth is carried out. In order to pursue an industrial scale-up of the growth process, commercially available precursors have been tested, namely: IBuGe, GeH_4, Si_2H_6 and $SnCl_4$. High crystalline quality SiGeSn layers lattice matched to Ge, with an excellent composition uniformity of 1% on 4 inch wafers, with maximum silicon and tin concentrations, of 3% and 0.9%, respectively, have been produced. Considering the material growth, new insights on the MOVPE SiGeSn growth process are presented, in particular by showing that: i) compared to GeH_4 and $SnCl_4$, Si_2H_6 is the gas source more influenced by the growth temperature, ii) there is a competition between Si_2H_6 and $SnCl_4$ which makes it difficult to incorporate Si in SiGeSn, as $SnCl_4$ partial pressure is increased, and iii) there is a possibility to get SiGeSn, Sn segregation/precipitation free, in the temperature range 480 °C–490 °C, by increasing the growth rate to values $>$ 7 nm/min and by exploiting the As carry-over produced by the previous III-V MOVPE runs. As adatoms on SiGeSn surface seem to play a similar role than the Si atoms incorporated in SiGeSn: they both facilitate Sn incorporation in the SiGeSn matrix, the former by limiting the exchange process between Ge and Sn on the surface, the latter by decreasing the compressive strain in the SiGeSn matrix [46]. Based on our theory, As adsorbed makes Sn segregation not energetically favourable, therefore Sn has two choices: i) either it stays in the bulk, or ii) it evaporates. On the other hand, when As is absent, there isn't any more an energetic barrier which hinder Sn segregation and the morphology deterioration can start from the beginning of the MOVPE deposition, By assuming that the bond length of adatoms determines the inhibiting role for Sn precipitation, we could explain why it is possible to grow SiGeSn layers Sn segregation free even at temperatures up to 490 °C, allowing to keep active the in-situ temperature wafer control during the MOVPE growth. Even if the new proposed surface-driven mechanism to suppress Sn segregation has to be confirmed by further experiments, by all means the demonstrated possibility to rise the SiGeSn growth temperature to value around 490 °C without morphology deterioration is a key feature to pursue an industrial scale up of the SiGeSn MOVPE growth process.

On the device aspect, an EQE value of about 70% has been measured for an InGaP/SiGeSn/Ge heterojunction filtered by a 0.4 μm thick GaAs cap layer. The device reaches 4% efficiency under G173-D spectrum, at 50x concentration. The EQE simulation carried out by considering the measured refractive index and absorption coefficient of the SiGeSn layer shows that the maximum EQE value, as well as the solar cell efficiency, are mainly limited by the high recombination velocity at the interface between InGaP and SiGeSn. We expect that this problem can be solved by reducing the SiGeSn surface porosity.

Owing to the remarkably higher absorption coefficient of SiGeSn with respect to Ge, the dilute SiGeSn considered in this study could be exploited both in TPV and space applications. In particular, since in a triple junction InGaP/InGaAs/Ge structure, Ge has shown poor resistance to proton radiation, especially in the case of low-energy protons (0.7 Mev) [47], SiGeSn could allow realizing devices more radiation resistance than Ge, owing the possibility to generate the some current with thinner layers. By all means, further efforts have to be addressed for a successful monolithic integration of SiGeSn in III-V based four junction solar cells, whose projected efficiency can reach 50% [45]. The following main further steps are for this purpose envisaged: i) obtain SiGeSn layers - Sn segregation free - still keeping the growth temperature $>$400 °C, with higher Si and Sn concentration, in order to increase the energy gap to 1eV, and with p-type polarity - ii) reduce SiGeSn surface porosity due to the presence of etch pit like defects, correlated with the Sn content in the samples.

The achievement of these objectives will allow fully exploiting the band gap engineering possibilities offered by the monolithic integration of III-V and IV compounds.

Credit author statement

Gianluca Timò: Conceptualization (lead); writing – original draft (lead); formal analysis (lead); writing – review and editing (equal), lead the MOVPE material growth activity.

Marco Calicchio: contribution to MOVPE growth activity.

Giovanni Abagnale: contribution to conceptualization and MOVPE growth activity.

Nicola Armani; contribution to material characterization methodology in particular on High Resolution X-Ray Diffraction and Secondary Ion-Mass Spectroscopy characterization, data analysis, review and editing.

Elisabetta Achilli: contribution to material characterization methodology in particular on High Resolution X-Ray Diffraction and Secondary Ion-Mass Spectroscopy characterization, data analysis.

Marina Cornelli: contribution to material characterization methodology in particular on Scanning Electron Microscope characterization and solar cell manufacturing.

Filippo Annoni: contribution to material characterization methodology in particular on Scanning Electron Microscope characterization and solar cell manufacturing.

Nicola Castagnetti: contribution to the device characterization methodology, in particular on current-voltage and spectral response characterization.

Maddalena Patrini: contribution to material characterization methodology, in particular on Atomic Force Microscope, Ellipsometry measurement and analysis, review and editing.

Lucio Claudio Andreani, contribution to spectral response simulation, review and editing.

Lucia Nasi; contribution to the material characterization methodology including Transmission Electron Microscopy, Selected Area Electron Diffraction, High Angle Annular Dark Field Scanning Transmission Electron Microscopy and High Energy Dispersive X-ray mapping, data analysis, review and editing.

Declaration of competing interest

The authors declare that they have no known competing financial interests or personal relationships that could have appeared to influence the work reported in this paper.

Acknowledgements

This research activity has been partially supported by the European H2020 project CPVMatch, "Concentrating Photovoltaic modules using advanced technologies and cells for highest efficiencies" under the GA 640873 and by the Research Fund for the Italian Electrical System in

compliance with the Decree of Minister of Economic Development April 16, 2018. We thank F.Trespidi and E.Malvisi from RSE for the device electrical characterization. A special thanks to Oliver Hoehn of Fraunhofer-Institute for Solar Energy for the support in the GaAs and InGaP MOVPE deposition, as well as to Peter Helm of RTG Mikroanalyse GmbH Berlin for SIMS measurements and analysis.

Appendix A. Supplementary data

Supplementary data to this article can be found online at https://doi.org/10.1016/j.solmat.2021.111016.

References

[1] B.R. Conley, H. Naseem, G. Sun, P. Sharps, S.Q. Yu, High efficiency MJ solar cells and TPV using SiGeSn materials, in: Conference Record of the IEEE Photovoltaic Specialists Conference, 2012, https://doi.org/10.1109/PVSC.2012.6317814.
[2] J. Kouvetakis, et al., Independently tunable electronic and structural parameters in ternary Group IV semiconductors for optoelectronic applications, Sci. Technol. 100 (2008) 4–8.
[3] R.A. Soref, C.H. Perry, Predicted band gap of the new semiconductor SiGeSn, J. Appl. Phys. 69 (1) (1991) 539–541, https://doi.org/10.1063/1.347704.
[4] N. Jain, et al., High-efficiency inverted metamorphic 1.7/1.1 eV GaInAsP/GaInAs dual-junction solar cells, Appl. Phys. Lett. 112 (5) (2018), https://doi.org/10.1063/1.5008517.
[5] J.F. Geisz, D.J. Friedman, J.M. Olson, S.R. Kurtz, B.M. Keyes, Photocurrent of 1eV GaInNAs lattice-matched to GaAs, J. Cryst. Growth 195 (1–4) (1998) 401–408, https://doi.org/10.1016/S0022-0248(98)00563-6.
[6] J. Xie, A.V.G. Chizmeshya, J. Tolle, V.R. Dcosta, J. Menendez, J. Kouvetakis, Synthesis, stability range, and fundamental properties of Si-Ge-Sn semiconductors grown directly on Si(100) and Ge(100) platforms, Chem. Mater. 22 (12) (2010) 3779–3789, https://doi.org/10.1021/cm100915q.
[7] S. Assali, J. Nicolas, O. Moutanabbir, Enhanced Sn incorporation in GeSn epitaxial semiconductors via strain relaxation, J. Appl. Phys. 125 (2) (2019), https://doi.org/10.1063/1.3645620.
[8] B. Vincent, et al., Undoped and in-situ B doped GeSn epitaxial growth on Ge by atmospheric pressure-chemical vapor deposition, Appl. Phys. Lett. 99 (15) (2011) 15–17, https://doi.org/10.1149/2.006305jss.
[9] S. Wirths, et al., Reduced pressure CVD growth of Ge and Ge1-xSnx alloys, ECS J. Solid State Sci. Technol. 2 (5) (2013) N99–N102, https://doi.org/10.1109/JPHOT.2010.2081357.
[10] J. Kouvetakis, J. Mathews, R. Roucka, A.V.G. Chizmeshya, J. Tolle, J. Menendez, Practical materials chemistry approaches for tuning optical and structural properties of group IV semiconductors and prototype photonic devices, IEEE Photonics J. 2 (6) (2010) 924–941, https://doi.org/10.1016/j.jcrysgro.2008.08.037.
[11] E. Welser, W. Guter, A. Wekkeli, F. Dimroth, Memory effect of Ge in III-V semiconductors, J. Cryst. Growth 310 (23) (2008) 4799–4802, https://doi.org/10.1063/1.4962096.
[12] T. Wilson, et al., Single and multi-junction solar cells utilizing a 1.0 eV SiGeSn junction, AIP Conf. Proc. 1766 (2016), https://doi.org/10.1109/CDE.2017.7905233.
[13] P. Cano, I. Lombardero, I. Rey-Stolle, A. Johnson, R. Hoffman, Multijunction solar cells incorporating group IV SiGeSn alloys, in: 2017 Spanish Conf. Electron Devices, 2017, pp. 1–3, https://doi.org/10.4229/EUPVSEC20152015-4CV.3.15.
[14] A.H. Soeriyadi, et al., A direct method of analysing the current matching condition in A multi-junction solar cell, in: 31st European Photovoltaic Solar Energy Conference and Exhibition, 2015, pp. 1456–1460, https://doi.org/10.1063/1.111495, no. 1.
[15] M. Dubey, et al., Growth of single crystal Ge films on GaAs and InGaP and highly oriented Au films on Ge, Appl. Phys. Lett. 2697 (64) (1994), https://doi.org/10.1063/1.111495.
[16] R. Jakomin, et al., P and n-type germanium layers grown using iso-butyl germane in a III-V metal-organic vapor phase epitaxy reactor, Thin Solid Films 519 (13) (2011) 4186–4191.
[17] G. Timò, et al., Novel approaches to MOVPE material deposition for high efficiency Multijunction Solar Cells, Cryst. Res. Technol. 49 (8) (2014) 606–613.
[18] G. Timò, N. Armani, G. Abagnale, B. Schineller, Advancement in the MOVPE technology to increase the process yield and expand the band gap engineering possibilities, in: 2014 IEEE 40th Photovoltaic Specialist Conference, PVSC, 2014, pp. 554–558, https://doi.org/10.1109/PVSC.2014.6924981.
[19] Y. Kim, et al., Highly efficient epitaxial Ge solar cells grown on GaAs (001) substrates by MOCVD using isobutylgermane, Sol. Energy Mater. Sol. Cells 166 (2017) 127–131, https://doi.org/10.1016/j.solmat.2017.03.015. March.
[20] R. Jia, T. Zhu, V. Bulović, E.A. Fitzgerald, Luminescence of III-IV-V thin film alloys grown by metalorganic chemical vapor deposition, J. Appl. Phys. 123 (17) (2018), https://doi.org/10.1063/1.5016443.
[21] D.V. Shenai, R.L. DiCarlo, M.B. Power, A. Amamchyan, R.J. Goyette, E. Woelk, Safer alternative liquid germanium precursors for relaxed graded SiGe layers and strained silicon by MOVPE, J. Cryst. Growth 298 (2007) 172–175, https://doi.org/10.1016/j.jcrysgro.2006.10.194. SPEC. ISS.
[22] M. Bosi, et al., Homoepitaxial growth of germanium for photovoltaic and thermophotovoltaic applications, J. Cryst. Growth 318 (1) (2011) 341–344, https://doi.org/10.1016/j.jcrysgro.2010.10.112.
[23] A. Salemi, Low Temperature Epitaxy Growth and Kinetic Modeling of SiGe for BiCMOS Application, 2011, https://doi.org/10.1016/j.jcrysgro.2006.10.194. *KTH master thesis*.
[24] S. Wirths, et al., "Low temperature RPCVD epitaxial growth of Si1−xGex using Si2H6 and Ge2H6, Solid State Electron. 83 (May 2013) 2–9, https://doi.org/10.1016/j.sse.2013.01.032.
[25] M. Bauer, et al., Synthesis of ternary SiGeSn semiconductors on Si(100) via SnxGe1-xbuffer layers, Appl. Phys. Lett. 83 (11) (2003) 2163–2165, https://doi.org/10.1063/1.1606104.
[26] J. Margetis, et al., Growth and characterization of epitaxial Ge1-x Snx alloys and heterostructures using a commercial CVD system, ECS Trans. 64 (6) (2014) 711–720, https://doi.org/10.1149/06406.0711ecst.
[27] P. Meunier-Beillard, et al., N2 as carrier gas: an alternative to H2 for enhanced epitaxy of Si, SiGe and SiGe:C,, Appl. Surf. Sci. 224 (1–4) (2004) 31–35, https://doi.org/10.1016/j.apsusc.2003.08.088.
[28] J. Kouvetakis, J. Menendez, A.V.G. Chizmeshya, TIN-BASED group IV semiconductors: new platforms for opto- and microelectronics on silicon, Annu. Rev. Mater. Res. 36 (1) (2006) 497–554, https://doi.org/10.1146/annurev.matsci.36.090804.095159.
[29] G. Attolini, et al., Homo and hetero epitaxy of Germanium using isobutylgermane, Thin Solid Films 517 (1) (2008) 404–406, https://doi.org/10.1016/j.tsf.2008.08.137.
[30] S.M. Gates, S.K. Kulkarni, Hydrogen coverage during Si growth from SiH4 and Si 2H6, Appl. Phys. Lett. 60 (1) (1992) 53–55, https://doi.org/10.1063/1.107371.
[31] J.M. Hartmann, J. Aubin, J.P. Barnes, A benchmark of germane and digermane for the low temperature growth of intrinsic and heavily in-situ boron-doped SiGe, ECS Trans. 75 (8) (2016) 281–293, https://doi.org/10.1149/07508.0281ecst.
[32] P. Aella, C. Cook, J. Tolle, S. Zollner, A.V.G. Chizmeshya, J. Kouvetakis, Optical and structural properties of Si xSn yGe 1-x-y alloys, Appl. Phys. Lett. 84 (6) (2004) 888–890, https://doi.org/10.1063/1.1645324.
[33] S. Wirths, et al., SiGeSn growth studies using reduced pressure chemical vapor deposition towards optoelectronic applications, Thin Solid Films 557 (2014) 183–187, https://doi.org/10.1016/j.tsf.2013.10.078.
[34] R. Khazaka, E. Nolot, J. Aubin, J.M. Hartmann, Growth and characterization of SiGeSn pseudomorphic layers on 200 mm Ge virtual substrates, Semicond. Sci. Technol. 33 (12) (2018) 124011, https://doi.org/10.1088/1361-6641/aaea32.
[35] J.-H. Fournier-Lupien, et al., In situ studies of germanium-tin and silicon-germanium-tin thermal stability, ECS Trans. 64 (6) (2014) 903–911, https://doi.org/10.1149/06406.0903ecst.
[36] Z. Zhang, J.S. Pan, J. Zhang, E.S. Tok, Kinetics of Ge diffusion, desorption and pit formation dynamics during annealing of Si0.8Ge0.2/Si(001) virtual substrates, Phys. Chem. Chem. Phys. 12 (26) (2010) 7171–7183, https://doi.org/10.1039/B927274G.
[37] C. Xu, et al., Synthesis and optical properties of Sn-rich Ge1-X -ySixSnymaterials and devices, Thin Solid Films 557 (2014) 177–182, https://doi.org/10.1016/j.tsf.2013.08.043.
[38] J. M, J.T. Nupur Bhargava, "As doping of Si – Ge – Sn epitaxial semiconductor materials on a commercial CVD reactor, Semicond. Sci. Technol. 32 (2017), https://doi.org/10.1088/1361-6641/aa7e19.
[39] E. Kasper, J. Werner, M. Oehme, S. Escoubas, N. Burle, J. Schulze, Growth of silicon based germanium tin alloys, Thin Solid Films 520 (8) (2012) 3195–3200, https://doi.org/10.1016/j.tsf.2011.10.114.
[40] V.Y. Lee, A. Sekiguchi, Organometallic Compounds of Low-Coordinate Si, Ge, Sn and Pb: From Phantom Species to Stable Compounds, 2010, ISBN 978-0-470-72543-6.
[41] N. Taoka, et al., Non-uniform depth distributions of Sn concentration induced by Sn migration and desorption during GeSnSi layer formation, Appl. Phys. Lett. 106 (6) (2015), https://doi.org/10.1063/1.4908121, 0–5.
[42] N.E.-D. Phoebe Pearce, Tom Wilson, Andrew Johnson, III-V multi-junction solar cells utilising group IV SiGeSn alloys as a 1.0 eV component sub-cell, in: 33rd European Photovoltaic Solar Energy Conference and Exhibition, 2017, pp. 1248–1252, https://doi.org/10.4229/EUPVSEC20172017-4CV.4.5.
[43] J. Vanjaria, et al., Growth of SiGeSn thin films using simplified PECVD reactor towards NIR sensor devices, ECS J. Solid State Sci. Technol. 9 (7) (2020), 074001, https://doi.org/10.1149/2162-8777/abaeb2.
[44] R. Roucka, et al., Demonstrating dilute-tin alloy SiGeSn for use in multijunction photovoltaics: single- and multijunction solar cells with a 1.0-eV SiGeSn junction, IEEE J. Photovoltaics (2016), https://doi.org/10.1109/JPHOTOV.2016.2559785.
[45] G. Timò, A. Martinelli, L.C. Andreani, A new theoretical approach for the performance simulation of multijunction solar cells, Prog. Photovoltaics Res. Appl. (2020) 1–16, https://doi.org/10.1002/pip.3225. October 2019.
[46] Y. Shimura, et al., EXAFS study of local structure contributing to Sn stability in SiyGe1-y-zSnz, November 2016, Mater. Sci. Semicond. Process. 70 (2017) 133–138, https://doi.org/10.1016/j.mssp.2016.11.013.
[47] R. Campesato, et al., NIEL DOSE and DLTS analyses on triple and single junction solar cells irradiated with electrons and protons, in: 2018 IEEE 7th World Conference on Photovoltaic Energy Conversion, WCPEC 2018 - A Joint Conference of 45th IEEE PVSC, 28th PVSEC and 34th EU PVSEC, 2018.